Clinical and Translational Report

Cell Metabolism

Mitochondrial Membrane Potential Identifies Cells with Enhanced Stemness for Cellular Therapy

Graphical Abstract

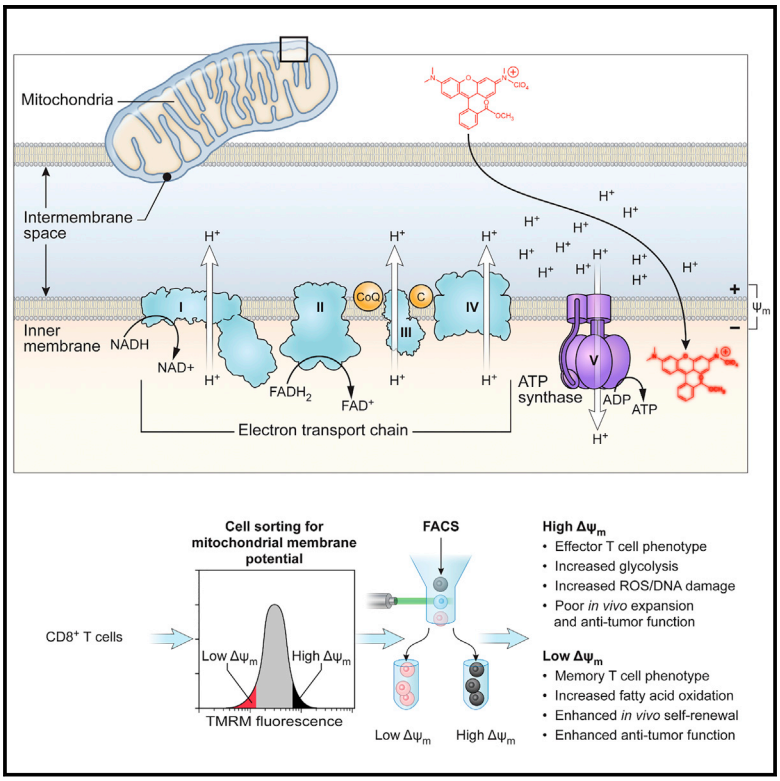

Highlights

- ΔΨm-based sorting segregates short-lived effector from memory T cell precursors
- Low-ΔΨm $CD8^+$ T cells demonstrate decreased oxidative stress
- Low-ΔΨm T cells demonstrate superior antitumor activity
- Low-ΔΨm marks self-renewing hematopoietic stem cells

Authors

Madhusudhanan Sukumar, Jie Liu, Gautam U. Mehta, ..., Pawel Muranski, Toren Finkel, Nicholas P. Restifo

Correspondence

sukumarm2@mail.nih.gov (M.S.), restifo@nih.gov (N.P.R.)

In Brief

Metabolic fitness is required for long-term function of T cells and HSC. Sukumar et al. describe a simple and clinically feasible method to isolate such metabolically robust cells, using a single parameter—mitochondrial membrane potential (ΔΨm)—for long-term survival, antitumor immunity, and hematopoietic reconstitution.

Accession Numbers

GSE67825
GSE74001

Sukumar et al., 2016, Cell Metabolism *23*, 63–76
January 12, 2016 ©2016 Elsevier Inc.
http://dx.doi.org/10.1016/j.cmet.2015.11.002

Mitochondrial Membrane Potential Identifies Cells with Enhanced Stemness for Cellular Therapy

Madhusudhanan Sukumar,[1,*] Jie Liu,[2] Gautam U. Mehta,[1] Shashank J. Patel,[1,3] Rahul Roychoudhuri,[1] Joseph G. Crompton,[1] Christopher A. Klebanoff,[1,4] Yun Ji,[5] Peng Li,[6] Zhiya Yu,[1] Greg D. Whitehill,[7] David Clever,[1,8] Robert L. Eil,[1] Douglas C. Palmer,[1] Suman Mitra,[6] Mahadev Rao,[9] Keyvan Keyvanfar,[7] David S. Schrump,[9] Ena Wang,[10] Francesco M. Marincola,[10] Luca Gattinoni,[5] Warren J. Leonard,[6] Pawel Muranski,[7] Toren Finkel,[2] and Nicholas P. Restifo[1,*]
[1]Center for Cancer Research, National Cancer Institute (NCI)
[2]Center for Molecular Medicine, National Heart, Lung, and Blood Institute (NHLBI)
National Institutes of Health (NIH), Bethesda, MD 20892, USA
[3]NIH-Georgetown University Graduate Partnership Program, Georgetown University Medical School, Washington, DC 20057, USA
[4]Clinical Investigator Development Program, NCI
[5]Experimental Transplantation and Immunology Branch, NCI
[6]Laboratory of Molecular Immunology and the Immunology Center, NHLBI
[7]Hematology Branch, NHLBI
NIH, Bethesda, MD 20892, USA
[8]Medical Scientist Training Program, The Ohio State University College of Medicine, Columbus, OH 43210, USA
[9]Thoracic and GI Oncology Branch, NCI, NIH, Bethesda, MD 20892, USA
[10]Sidra Medical and Research Center, Doha, Qatar
*Correspondence: sukumarm2@mail.nih.gov (M.S.), restifo@nih.gov (N.P.R.)
http://dx.doi.org/10.1016/j.cmet.2015.11.002

SUMMARY

Long-term survival and antitumor immunity of adoptively transferred CD8$^+$ T cells is dependent on their metabolic fitness, but approaches to isolate therapeutic T cells based on metabolic features are not well established. Here we utilized a lipophilic cationic dye tetramethylrhodamine methyl ester (TMRM) to identify and isolate metabolically robust T cells based on their mitochondrial membrane potential ($\Delta\Psi$m). Comprehensive metabolomic and gene expression profiling demonstrated global features of improved metabolic fitness in low-$\Delta\Psi$m-sorted CD8$^+$ T cells. Transfer of these low-$\Delta\Psi$m T cells was associated with superior long-term in vivo persistence and an enhanced capacity to eradicate established tumors compared with high-$\Delta\Psi$m cells. Use of $\Delta\Psi$m-based sorting to enrich for cells with superior metabolic features was observed in CD8$^+$, CD4$^+$ T cell subsets, and long-term hematopoietic stem cells. This metabolism-based approach to cell selection may be broadly applicable to therapies involving the transfer of HSC or lymphocytes for the treatment of viral-associated illnesses and cancer.

INTRODUCTION

Immunotherapy using adoptive transfer of tumor-specific T cells mediates durable and complete disease regression in some patients with metastatic cancer (Brentjens et al., 2013; June et al., 2015; Porter et al., 2011; Riddell and Greenberg, 1995). Mounting evidence has shown that metabolism supports and drives many basic features of T cells, including cellular activation, proliferation, differentiation, effector function (Gerriets et al., 2015; Gerriets and Rathmell, 2012; MacIver et al., 2013; Michalek et al., 2011a, 2011b; Pearce et al., 2009, 2013; Sena et al., 2013; Shi et al., 2011), and antitumor immunity. This has led to a growing interest in leveraging this understanding to improve the efficacy of T cell transfer therapies, such as adoptive transfer immunotherapy in the treatment of cancer. In preclincial models it has been shown that highly glycolytic T cells are short-lived after adoptive transfer and have impaired antitumor immunity (Sukumar et al., 2013), whereas T cells with a metabolic profile characterized by elevated fatty acid oxidation (FAO) (Pearce et al., 2009) and enhanced mitochondrial spare respiratory capacity (SRC) have greater long-term survival (van der Windt et al., 2012).

Although there is increasing evidence that metabolism can affect the survival and antitumor function of T cells, identifying a simple and clinically feasible method to isolate T cells with favorable metabolic features has proved challenging. Because mitochondria are the central metabolic organelle in cells, we hypothesized that the measurement of a single mitochondrial-associated parameter may help to identify T cells with a favorable bioenergetic profile that can survive in vivo for long periods after adoptive transfer for T cell-based immunotherapy.

Here, we describe a clinically feasible method to isolate functionally robust T cells based on a single metabolic parameter: mitochondrial membrane potential ($\Delta\Psi$m). Mitochondria produce energy by establishing an electrochemical proton motive force (Δp) across their inner cell membrane, which in turn fuels the synthesis of ATP by driving the proton turbine F0F1 ATPase (Ehrenberg et al., 1988; Sena et al., 2013; Wang and Green, 2012; Weinberg et al., 2015). We show that CD8$^+$ T cells that are found to have low-$\Delta\Psi$m display enhanced in vivo persistence, augmented autoimmunity, and greater antitumor

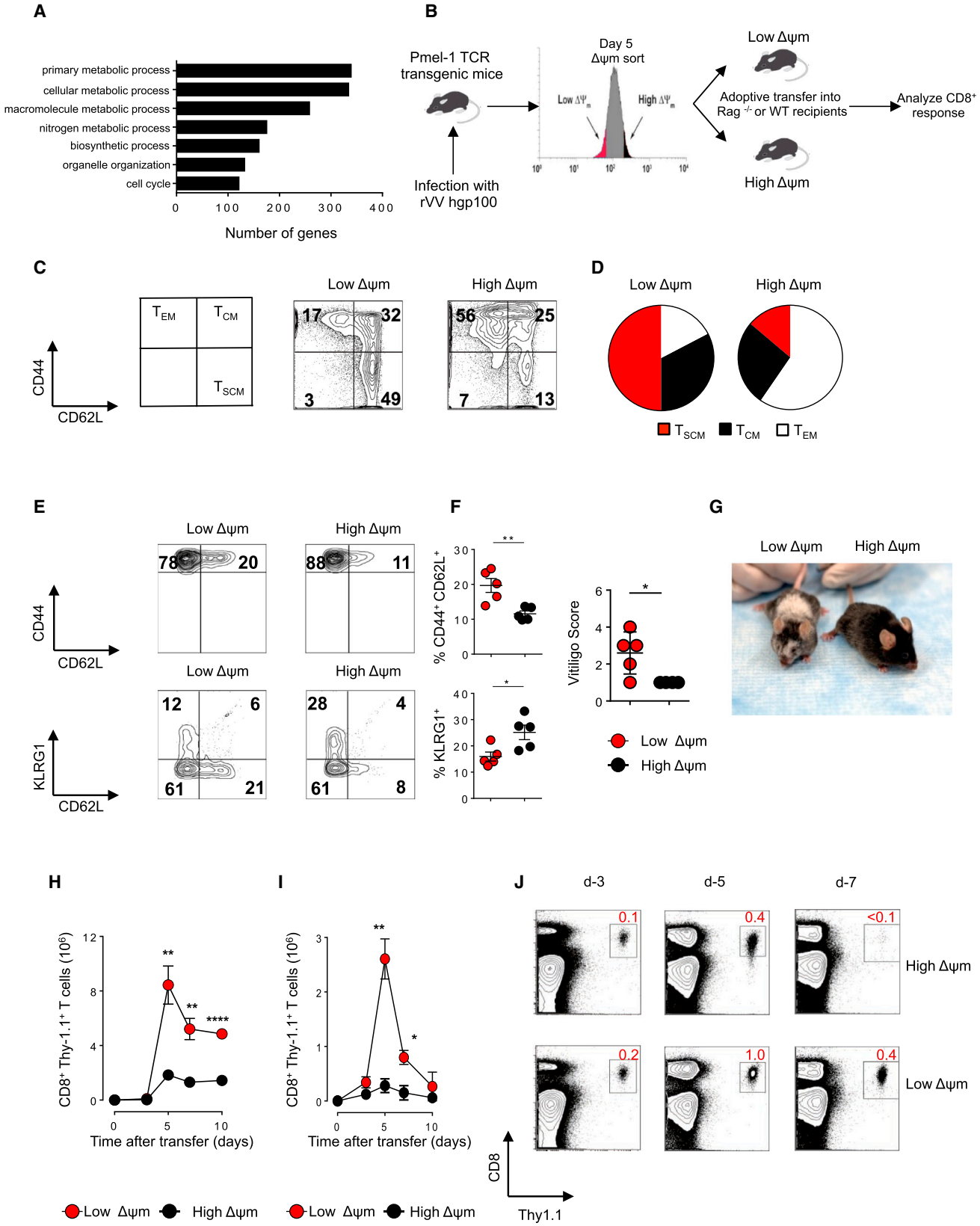

(legend on next page)

immunity relative to high-ΔΨm cells. These findings demonstrate that metabolic sorting can complement sorting based on conventional cell surface markers in identifying cells with the capacity for long-term survival and ongoing effector function after adoptive transfer. This immunometabolomic approach to cell sorting may have important and immediate therapeutic applications in enhancing cell-based therapies for patients with viral-associated illness, advanced cancer, and disorders of hematopoiesis.

RESULTS AND DISCUSSION

ΔΨm-Based Sorting Segregates Short-Lived Effector from Memory T Cell Precursors

To understand the molecular programs regulating long-term persistence and antitumor functions of the CD62L$^+$ memory T cell population, we compared a genome-wide microarray analysis of minimally differentiated stem-cell memory T cells ($T_{SCM,}$ CD62L$^+$CD44$^-$Sca-1$^+$) with more highly differentiated effector memory T cells ($T_{EM,}$ CD62L$^-$CD44$^+$) and found significant differences in the expression of genes related to metabolic processes (Figure 1A; see Table S1 available online). We then FACS-purified T cells using the mitochondrial potential-sensitive dye TMRM, a lipophilic cationic dye that accumulates in the mitochondrial matrix in proportion to the magnitude of ΔΨm electronegativity (Ehrenberg et al., 1988). We vaccinated pmel-1 T cell receptor (TCR) transgenic mice, whose CD8$^+$ T cells recognize an epitope derived from the shared melanocyte/melanoma differentiation antigen (Ag) gp100, with a recombinant vaccinia virus encoding hgp100 (gp100-VV). At the peak of the primary immune response following vaccination, we FACS-sorted the bulk population of T cells into low-ΔΨm and high-ΔΨm fractions and subsequently transferred equal numbers of cells into either wild-type (WT) or (recombination activating gene-2) *Rag2*$^{-/-}$ recipient mice, which were then infected with gp100-VV (Figure 1B). Cells derived from the low-ΔΨm cell fraction were enriched in T_{SCM} and central memory ($T_{CM,}$ CD62L$^+$CD44$^+$) subsets compared to cells derived from the high-ΔΨm fraction, which was composed predominantly of effector memory T cells (T_{EM}) (Figures 1C and 1D). Upon adoptive transfer, a higher proportion of low-ΔΨm cells retained a CD62L$^+$ CD44$^+$ T_{CM} phenotype, whereas a greater proportion of high-ΔΨm CD8$^+$ T cells underwent terminal differentiation, as revealed by loss of the memory marker (CD62L) and concomitant acquisition of the senescence marker (Killer cell lectin-like receptor subfamily G member 1) KLRG-1 (Figures 1E and 1F). We have previously demonstrated a correlation between the degree of vitiligo and long-term persistence of CD8$^+$ T cells (Palmer et al., 2008). Therefore, we analyzed the degree of vitiligo in *Rag2*$^{-/-}$ recipient mice after adoptive transfer of low-ΔΨm and high-ΔΨm subsets. The on-target autoimmune vitiligo observed in mice which received low-ΔΨm CD8$^+$ T cells was significantly more severe compared with animals that received high-ΔΨm CD8$^+$ T cells (Figure 1G).

We next activated pmel-1 CD8$^+$ T cells with cognate antigen in vitro to induce effector differentiation and isolated activated T cells based on ΔΨm by FACS sorting (Figure S1A). Phenotypic analyses revealed that both low-ΔΨm and high-ΔΨm CD8$^+$ T cells showed evidence of activation compared with unstimulated naive T cells (Figure S1B). Additionally, CD62L was highly expressed in low-ΔΨm CD8$^+$ T cells compared with high-ΔΨm CD8$^+$ T cells (Figures S1C and S1D). Levels of perforin were unchanged (Figure S1E), whereas Granzyme B was expressed at reduced levels in the low-ΔΨm CD8$^+$ T cell subset (Figure S1F). To test whether low-ΔΨm CD8$^+$ T cells differ in their proliferation, we activated the CD8$^+$ T cells for 4 days and evaluated Ki-67 staining as a measure of CD8$^+$ T cell proliferation. We found that the low-ΔΨm CD8$^+$ T cells proliferated less compared with the high-ΔΨm CD8$^+$ T cells (Figure S1G). Next, we sought to ascertain whether differences in ΔΨm affected the expansion in a secondary response, as memory T cells can undergo robust expansion during a recall response and demonstrate long-term persistance (Graef et al., 2014; Kaech and Cui, 2012). We adoptively transferred low-ΔΨm and high-ΔΨm pmel-1 cells into wild-type (WT) or lymphodeplete hosts. We have previously shown that lymphodepletion before adoptive cell transfer (ACT) can dramatically improve the antitumor efficacy and persistence of transferred T cells (Gattinoni et al., 2005). Furthermore, in the most recent clinical trials, lymphodepletion preceding ACT results in an objective response rate of 50% in patients with solid metastatic melanomas (Restifo et al., 2012). Following transfer, recipient mice were infected with gp-100-VV. Low-ΔΨm T cells demonstrated robust expansion following adoptive transfer, whereas transfer of equal numbers of high-ΔΨm cells resulted in relatively poor in vivo expansion in both lymphodepleted mice (Figure 1H) and WT recipients (Figure 1I). Low-ΔΨm cells showed enhanced survival capacity, as evidenced by the frequency of congenically marked T cells in the spleens of vaccinated mice after transfer (Figures 1J and S1H). Low-ΔΨm and high-ΔΨm CD8$^+$ T cells exhibited increased production of IFN-γ and TNF-α indicating that both subsets exhibit full effector function in vivo at the peak of the immune response (Figure S1I). We conclude that

Figure 1. ΔΨm-Based Sorting Segregates Short-Lived Effector from Memory T Cell Precursors

(A) Gene ontology analysis from microarray data shows several differentially expressed genes associated with metabolism in T_{SCM} (CD8$^+$CD44$^-$CD62L$^+$Sca-1$^+$) versus T_{EFF} (CD8$^+$CD44$^+$CD62L$^-$).

(B) Schematic for sorting based on ΔΨm.

(C) Flow cytometric analysis of CD44 and CD62L in splenocytes isolated from Pmel mice 5 days after rVVhgp100 infection in indicated ΔΨm subsets.

(D) Pie charts depicting the proportion of T_{SCM}, T_{CM}, and T_{EFF} CD8$^+$ T cell subsets in indicated ΔΨm subsets.

(E and F) (E) Flow cytometry and (F) quantification of memory (CD62L) and senescence (KLRG1) markers in adoptively transferred cells isolated from spleen of wild-type mice 5 days after adoptive transfer of 10^5 Thy1.1$^+$ CD8$^+$ T cells of indicated ΔΨm subset.

(G) Vitiligo score of *Rag*$^{-/-}$ mice 6 months after adoptive transfer of 10^5 Thy1.1$^+$ CD8$^+$ T cells of indicated ΔΨm subsets.

(H) Kinetic analysis of adoptively transfered Thy1.1$^+$ CD8$^+$ T cells of each indicated ΔΨm subset (10^5 per group) into irradiated (lymphodepleted) B6 mice.

(I and J) (I) Kinetic analysis of adoptively transfered Thy1.1$^+$ CD8$^+$ T cells of each indicated ΔΨm subset (10^5 per group) into nonirradiated (lymphoreplete) B6 mice and (J) flow cytometric analysis of adoptively transfered Thy1.1$^+$ CD8$^+$ T cells of each indicated ΔΨm subset (10^5 per group) into nonirradiated (lymphoreplete) B6 mice.

Data are presented as mean ± SEM and *$p < 0.05$; **$p < 0.01$; ****$p < 0.0001$ (two-tailed t test).

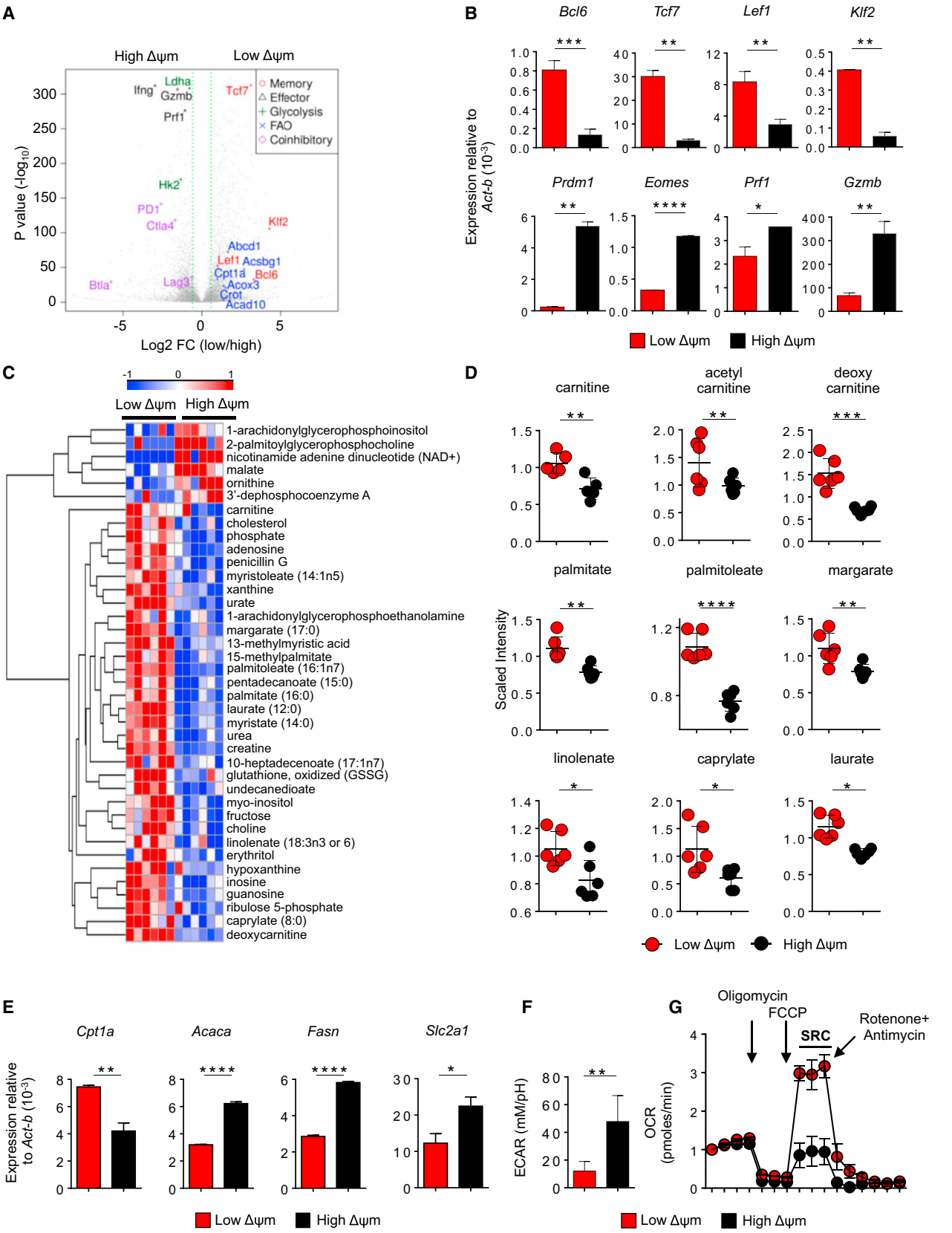

(legend on next page)

sorting primed T cells based on low-ΔΨm identifies a population of cells with an enhanced capacity to expand, persist, and mediate on-target immunity relative to cells with high ΔΨm.

Low-ΔΨm Cells Display a Gene Expression and Metabolic Profile of Memory CD8$^+$ T Cells

Using RNA-seq analysis to provide a global assessment of differential gene expression between ΔΨm subsets, we identified a total of 1,895 genes that were differentially expressed (1,151 upregulated and 744 downregulated) in the low-ΔΨm compared to high-ΔΨm fractions (Figure 2A; Table S2). Low-ΔΨm cells were specifically enriched for the expression of genes encoding factors known to promote memory CD8$^+$ T cell formation, including B cell CLL/lymphoma 6 (*Bcl6*), the Wnt-β-catenin signaling transducers transcription factor 7 (*Tcf7*) and lymphoid enhancer factor (*Lef1*), and the FOXO-target gene Kruppel-like factor 2, lung (*Klf2*) (Figure 2A). Quantitative PCR analyses confirmed these differences in gene expression (Figure 2B). In contrast, transcripts encoding key regulators of effector differentiation such as PR domain zinc finger protein 1 (*Prdm1*) and eomesodermin (*Eomes*) were enriched in high-ΔΨm cells. Furthermore, genes that encode for cytotoxic effector molecules such as perforin (*Prf1*) and granzyme B (*Gzmb*) were also enriched within the high-ΔΨm subset (Figure 2B). We also found that multiple distinct inhibitory T cell receptors such as programmed death-1 (PD-1), cytotoxic T-lymphocyte-associated protein 4 (CTLA-4), B- and T-lymphocyte attenuator (BTLA), and lymphocyte-activation gene 3 (LAG-3) were enriched in the high-ΔΨm subset compared with the low-ΔΨm subset (Figure 2A).

Recent studies have demonstrated that metabolic programs may in part determine memory and effector CD8$^+$ T cell fate (MacIver et al., 2013; Pearce et al., 2009; Sukumar et al., 2013). To elucidate the metabolic program associated with low-ΔΨm CD8$^+$ T cells, we performed an unbiased metabolomic profiling of sorted ΔΨm subsets. This metabolic fingerprinting revealed that ΔΨm CD8$^+$ subsets had differences in 39 distinct metabolic intermediates (Figure 2C). Relative levels of ribose-5-phosphate, sedoheptulose-5-phosphate, and ribulose-5-phosphate were measured in the low-ΔΨm and high-ΔΨm CD8$^+$ T cell subsets using LC/MS, but only ribulose-5-phosphate levels were significantly different (Figure S2A). Notably, multiple carnitine species were more abundant in low-ΔΨm cells compared to their high-ΔΨm counterparts (Figure 2D). In addition, we measured increased levels of short-, medium-, and long-chain free fatty acid (FFA) metabolites in the low-ΔΨm subset (Figure 2D).

Given the importance of the balance between FAO and fatty acid synthesis (FAS) on T cell differentiation (Berod et al., 2014), we next evaluated whether low-ΔΨm cells display differences in the expression of key enzymes involved in FAS and FAO. Low-ΔΨm cells displayed increased expression of carnitine palmitoyl transferase 1a (*Cpt1a)*, the rate-limiting enzyme involved in transport of fatty acids into the mitochondria for subsequent β-oxidation (van der Windt et al., 2012) (Figure 2E). Additionally, the expression of both acetyl-coA-carboxylase (*Acaca*) and fatty acid synthase (*Fasn*) was reduced in the low-ΔΨm subset. These data indicate that low-ΔΨm cells may preferentially engage in FAO as opposed to FAS (Figure 2E). RNA-Seq analysis revealed that gene expression of many of the enzymes involved in the glucose metabolism such as hexokinase 2 (*Hk2*), lactate dehydrogenase (*Ldha*), pyruvate dehydrogenase (*Pdh*), and pyruvate dehydrogenase kinase, isoform 2 (*Pdk2*), are differentially expressed between the low-ΔΨm and high-ΔΨm CD8$^+$ T cell groups (Table S2). Quantitative PCR analysis confirmed that low-ΔΨm cells displayed reduced expression of both *Hk2* and *Ldha* (Figure S2B). Interestingly, RNA-seq analysis revealed that *Pdk1* expression was not significantly altered in ΔΨm subsets, and quantitative PCR analysis revealed that the expression of *Pdk2* was also not significantly increased in low-ΔΨm CD8$^+$ T cells (Figure S2B). The high-ΔΨm subset expressed greater levels of the glucose transporter solute carrier family 2, facilitated transporter member 1 (*Slc2a1*) (Figure 2E). To determine whether these gene expression and metabolic measurements were associated with functional changes in cellular metabolism, we next evaluated the extracellular acidification rate (ECAR), which quantifies proton production as a surrogate for lactate production and thus reflects glycolytic flux and the oxygen consumption rate (OCR), a measure of overall mitochondrial respiration. Consistent with gene expression data, high-ΔΨm cells demonstrated evidence of increased glycolytic flux (Figure 2F). These cells also exhibited greater basal OCR (Figure S2C). Low-ΔΨm cells exhibited greater spare respiratory capacity, a feature of long-lived memory CD8$^+$ T cells (van der Windt et al., 2012) (Figure 2G). Thus, low-ΔΨm cells exhibit many of the metabolic hallmarks associated with memory T cells, including increased expression of *Cpt1a* and increased levels of free fatty acids, increased spare respiratory capacity, and relatively low glycolytic flux. Taken together, we conclude that sorting T cells based solely on ΔΨm identifies cell populations with distinct gene and metabolic profiles associated with either effector T cell (high-ΔΨm) or long-lived memory (low-ΔΨm) T cell subsets.

Low ΔΨm Defines Stem-Cell-like Activity in an Array of Cell Types

Given that ΔΨm-based sorting allowed for the enrichment of CD8$^+$ T cells with distinct metabolic and in vivo functional activities, we hypothesized that this strategy might have a similar

Figure 2. Low-ΔΨm Cells Display a Gene Expression and Metabolic Profile of Memory CD8$^+$ T Cells

(A) Volcano plot of RNA-sequencing analysis of ΔΨm-sorted CD8$^+$ T cell subsets. Analysis includes a total of 1,895 genes that were either upregulated (1,151 genes) or downregulated (744) by at least a 2-fold change. Highlighted are canonical genes associated with glycolysis, fatty acid oxidation (FAO), effector, memory differentiation, and coinhibitory receptors.

(B) Bar graphs showing quantitative RT-PCR expression of indicated memory and effector genes in CD8$^+$ T cells.

(C) Global metabolomic heatmap showing metabolites detected in CD8$^+$ T cells within ΔΨm subsets.

(D) Scatterplot showing quantification of key metabolites (FAO) in CD8$^+$ T cells from the indicated ΔΨm subset.

(E) Bar graphs showing quantitative RT-PCR analysis for expression of *Cpt1a*, *Acaca*, *Fasn*, and *Slc2a1* within ΔΨm subsets.

(F) ECAR of low-ΔΨm and high-ΔΨm CD8$^+$ T cells.

(G) OCR of low-ΔΨm and high-ΔΨm CD8$^+$ T cells in response to indicated mitochondrial modulators: oligomycin; FCCP, R&A-rotenone and antimycin A.

Data are presented as mean ± SEM and *$p < 0.05$; **$p < 0.01$; ***$p < 0.001$; ****$p < 0.0001$ (two-tailed t test).

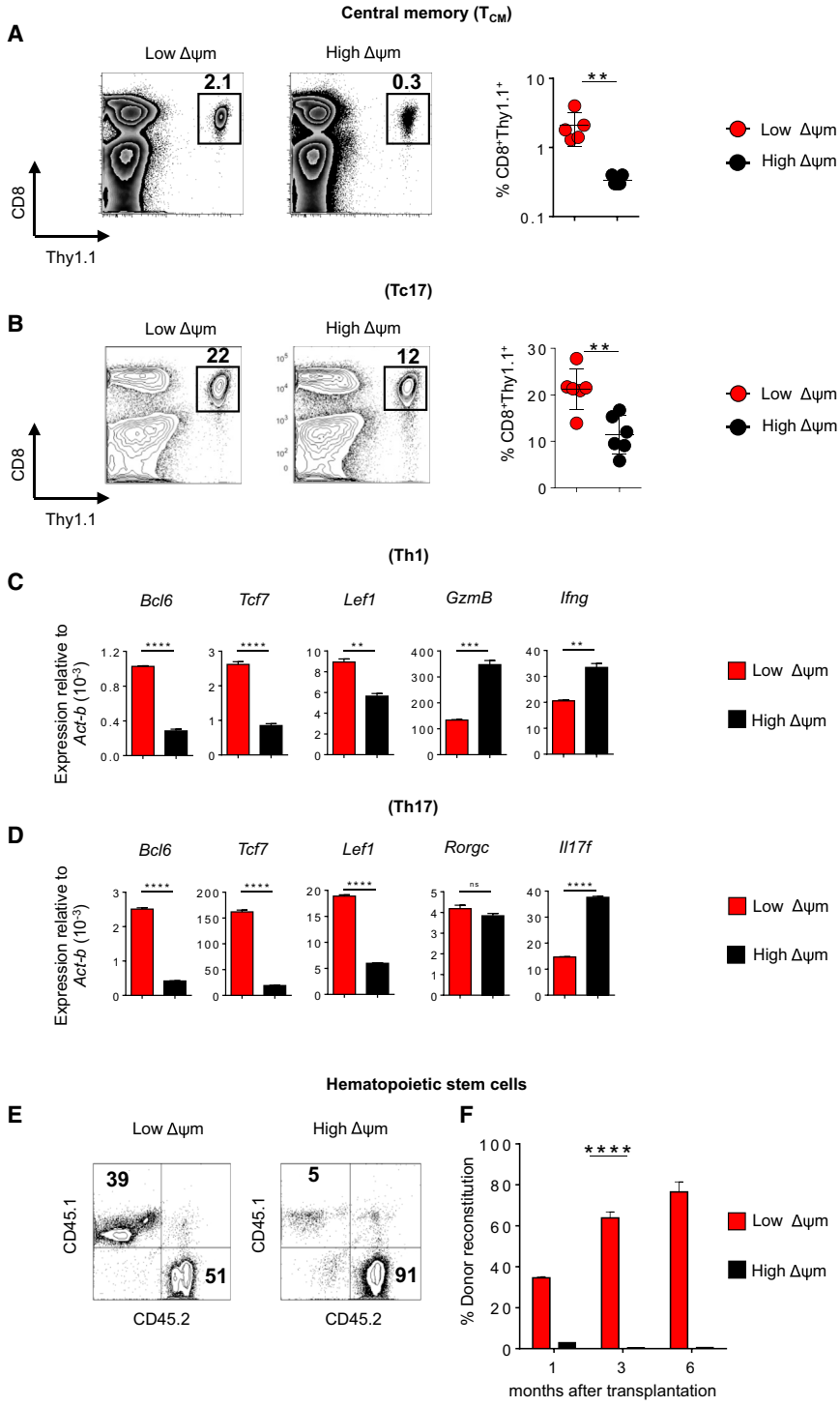

Figure 3. Stem-like Characteristics of Low-ΔΨm Cells Are Conserved within Other Cell Types

(A and B) Flow cytometic analysis after adoptive transfer of 10^5 high-ΔΨm or low-ΔΨm $CD8^+$ T cells isolated from spleen of B6 mice.

(C and D) Bar graphs showing expression of quantitative RT-PCR analysis of indicated genes in Th1 (C) and Th17 cells (D) $CD4^+$ T cells in indicated ΔΨm subsets.

(E) Representative contribution of sorted donor mouse HSCs (CD45.1) mixed with competitor bone marrow (CD45.2) at 1 month (F) and over a 6 month period (n = 5 mice per group).

Data are presented as mean ± SEM and $^{**}p < 0.01$; $^{***}p < 0.001$; $^{****}p < 0.0001$ (two-tailed t test).

discriminatory power in a variety of other cell types, including T cell subsets and hematopoietic stem cell (HSC). A recent report demonstrated that adult tissue memory T cells with stem cell-like properties reside within the $CD62L^+$ T_{CM} population (Graef et al., 2014). Therefore, using a gating strategy based on T_{CM} surface markers ($CD8^+CD44^+CD62L^+$), we further partitioned the T_{CM} subset into low-ΔΨm and high-ΔΨm T_{CM} populations (Figures S3A and S3B). We found that low-ΔΨm T_{CM} display increased mRNA levels of transcription factors and genes associated with memory precursors (Figure S3C). Following adoptive transfer, low-ΔΨm T_{CM} demonstrated a 6-fold greater engraftment in the spleen of vaccinated mice compared with their high-ΔΨm counterparts (Figure 3A). Thus, we were able to isolate a functionally distinct fraction of stem-cell-like T cells from an otherwise phenotypically homogenous T_{CM} population. We next addressed whether ΔΨm sorting would allow us to isolate metabolically fit T cells within distinct effector T cell populations (Tc17, Th1, and Th17 cells). We generated Tc17 cells and segregated them based on ΔΨm by FACS sorting (Figure S3D). Upon adoptive transfer, we found that low-ΔΨm Tc17 cells displayed enhanced survival capacity compared with their high-ΔΨm counterparts (Figure 3B). Similarly, using $CD4^+$ cells specific for the tissue differentiation antigen TRP-1 (Muranski et al., 2011), we polarized T cells under Th1 and Th17 conditions and segregated them into low-ΔΨm and high-ΔΨm (Th1 and Th17) subsets. Again expression of factors known to promote longevity, including *Bcl6*, *Tcf7*, and *Lef1*, were enriched in the low-ΔΨm fraction relative to the high-ΔΨm fraction within these effector $CD4^+$ subsets (Figures 3C and 3D).

There is a growing appreciation that intracellular metabolism may be critical for the maintanence of HSC and induced pluripotent stem cells (iPSCs) (Folmes et al., 2011; Ito et al., 2012; Simsek et al., 2010; Takubo et al., 2010), embryonic stem cells (Schieke et al., 2008), and cancer stem cells (CSCs) (Ye et al., 2011). To determine whether this metabolic sorting has applicability in stem cells, we analyzed long-term hematopoietic stem cells (LT-HSC) purified from mouse bone marrow based on conventional surface markers ($Lin^-/Sca1^+/c\text{-}kit^+/CD34^-$). We isolated

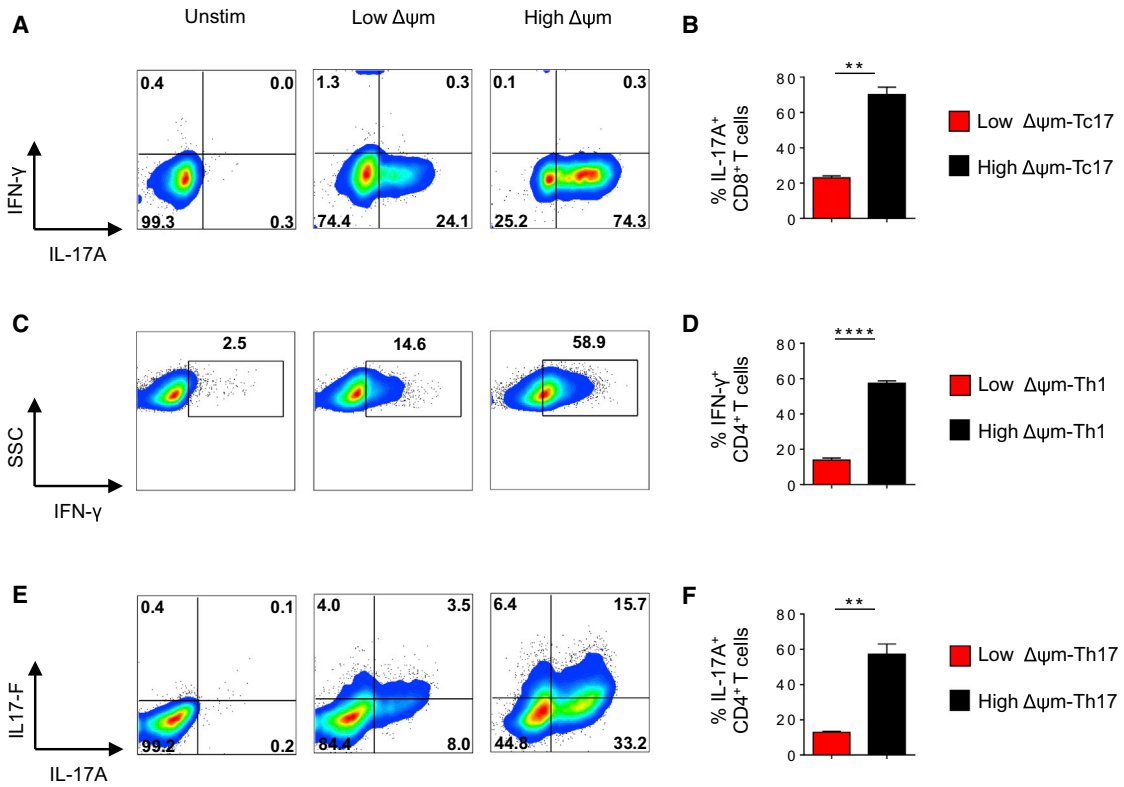

Figure 4. High-ΔΨm Is Associated with Effector Cytokine Production in T Cells

(A and B) (A) Representative intracellular staining and (B) quantification of IL-17A by Tc17 polarized Pmel-1 $CD8^+$ cells generated in vitro after 4 hr restimulation with phorbol myrystate acetate (PMA) and ionomycin in the presence of brefeldin A.

(C and D) (C) Representative intracellular staining and (D) quantification of IFN-γ by Th1 TRP-1 $CD4^+$ cells generated in vitro.

(E and F) (E) Representative intracellular staining of IL-17A and IL-17F and (F) quantification of IL-17A by Th17-polarized TRP-1 $CD4^+$ cells generated in vitro. Data are presented as mean ± SEM and $^{**}p < 0.01$; $^{****}p < 0.0001$ (two-tailed t test).

mouse LT-HSC and characterized the phenotype of the corresponding low-ΔΨm and high-ΔΨm subsets (Figure S4A). Several reports have demonstrated that CD150 high HSCs are associated with greater self-renewal and long-term reconstitution potential (Morita et al., 2010). Therefore, we evaluated the expression of CD150 expression in the low-ΔΨm and high-ΔΨm HSCs. We found that CD150, a LT-HSC-self renewal marker, was expressed by 80% of the low-ΔΨm HSC population, while high-ΔΨm HSCs did not express any levels of this marker (Figures S4B and S4C). We next purified low-ΔΨm and high-ΔΨm subsets from within mouse $Lin^-/Sca1^+/c\text{-}kit^+/CD34^-$ cells and mixed these with competitor bone marrow prior to reinfusion into lethally irradiated recipient mice. As measured by donor reconstitution, long-term engraftment capacity of low-ΔΨm LT-HSCs was significantly more robust than high-ΔΨm LT-HSCs (Figures 3E and 3F). Our results support the view that sorting HSC based on ΔΨm can identify long-term self-renewing HSC for transplant capable of effective long-term repopulation.

High ΔΨm Is Associated with Effector Cytokine Production in T Cells

We sought to determine whether ΔΨm can modulate cytokine production in effector T cell subsets. To test this, we generated effector T cell subsets such as Tc17, Th1, and Th17; further sorted these subsets into low-ΔΨm and high-ΔΨm subsets; and measured cytokine production within each lineage. High-ΔΨm Tc17 secreted 3-fold higher levels of IL-17A compared with the low-ΔΨm Tc17 subset (Figures 4A and 4B). Furthermore, under Th1-polarizing conditions high-ΔΨm Th1 $CD4^+$ T cells demonstrated a 4-fold increase in levels of IFN-γ compared with the low-ΔΨm Th1 subset (Figures 4C and 4D). Finally, the majority of high-ΔΨm Th17 cells expressed increased levels of both IL-17A and IL-17F compared to their low-ΔΨm counterparts (Figures 4E and 4F). These results suggest that an increase in ΔΨm is associated with increased effector cytokine secretion in a variety of lymphocyte lineages. Together, these data show that in addition to inducing aerobic glycolysis, lymphocytes also may need to increase their ΔΨm to achieve full effector cytokine production and function.

Low-ΔΨm $CD8^+$ T Cells Demonstrate Decreased Oxidative Stress

The functional demands and longevity of stem cell-like memory T cells likely require programs to reduce oxidative stress and maintain long-term genomic stability. We therefore tested if the increased functionality observed in low-ΔΨm $CD8^+$ T cells might reflect an intrinsic reduction in oxidative stress levels. Direct reduction of ΔΨm in $CD8^+$ T cells resulted in reduced ROS levels

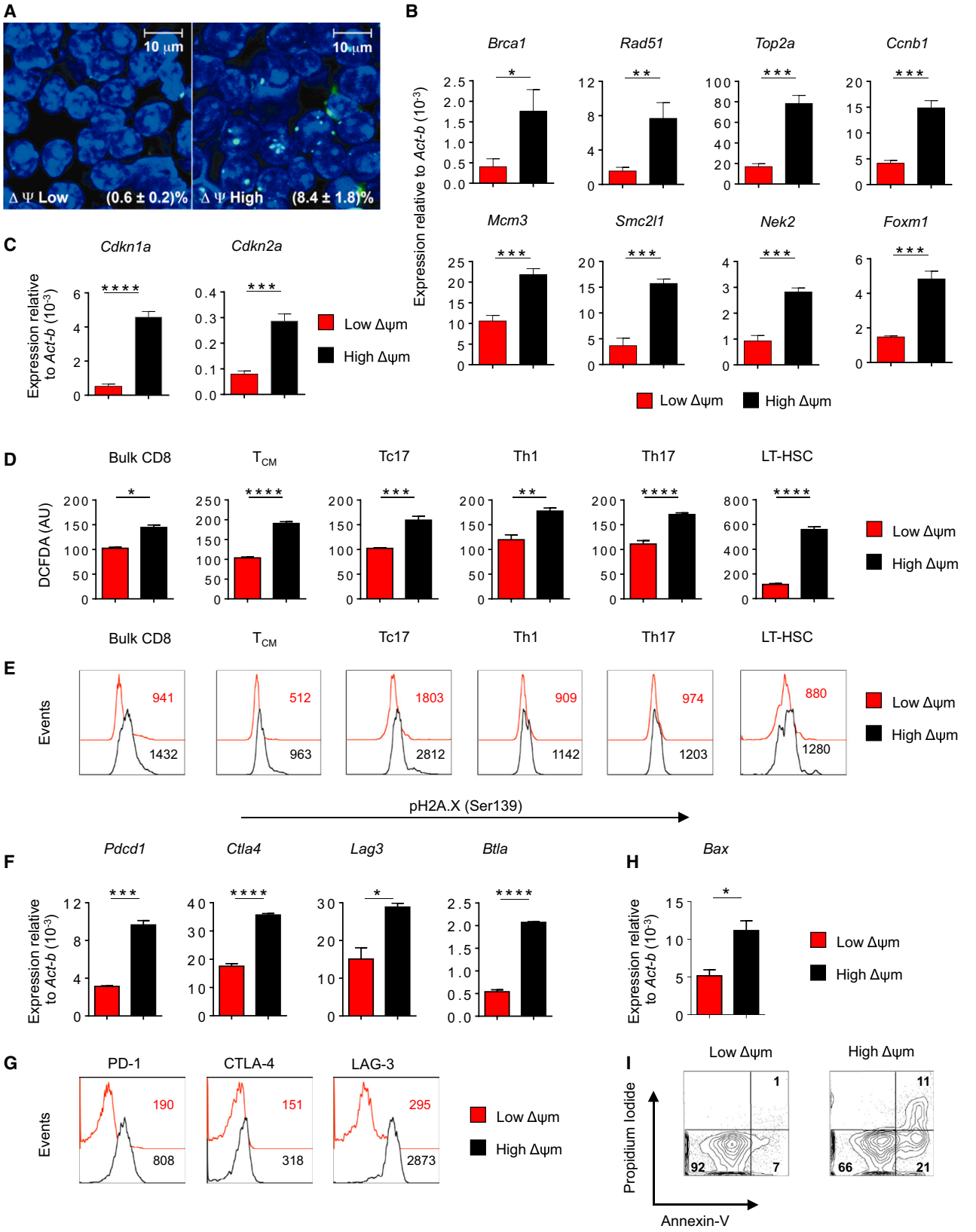

(legend on next page)

as measured by the redox-sensitive fluorophore dihydrodichlorofluorescein diacetate (DCFDA) (Figure S4D). Low-ΔΨm CD8$^+$ T cells had a large reserve pool of oxidized glutathione (GSSG) compared with high-ΔΨm CD8$^+$ T cells (Figure S4E). Furthermore, the low-ΔΨm CD8$^+$ T cells also maintained increased mRNA expression of ROS-detoxifying enzymes including catalase (*Cat*), glutathione peroxidase 4 (*Gpx4*), superoxide dismutase 1 (*Sod1*), and superoxide dismutase 2 (*Sod2*) (Figure S4F) that may contribute to low-ΔΨm CD8$^+$ T cell redox regulation. The increased levels of glutathione and antioxidant genes may help to support the in vivo expansion and redox balance of low-ΔΨm CD8$^+$ T cells. These cells also had reduced levels of DNA damage, as assessed by Ser139 phosphorylated histone varant H2A.X (γH2AX) foci formation on nuclear DNA (Figure 5A). In contrast, high-ΔΨm T cells exhibited increased γH2AX staining, and demonstrated relative upregulation of genes involved in DNA replication, DNA repair (Figure 5B), and cell-cycle arrest (Figure 5C).

To test if the hypothesis that ROS generation may compromise function of self-renewal and longevity programs is generalizable to other T cell subsets and to HSC, we measured whether increased ROS and DNA damage levels were present within high-ΔΨm subsets in varieties of other cell types. Consistent with findings using bulk activated CD8$^+$ T cells, we found that the high-ΔΨm subset of the central memory CD8$^+$ T cell subset (T_{CM}), effector T cell subsets (Tc17, Th1, and Th17 cells), and LT-HSC exhibited elevated ROS levels (Figure 5D) and DNA damage (Figure 5E) compared to their low-ΔΨm counterparts. Elevated levels of oxidative stress and damaged DNA resulting from increased ROS in stem cells have been linked with impaired stem cell self-renewal (Suda et al., 2011). Our results are consistent with a model in which high continuous and unregulated levels of ROS may limit the long-term survival of lymphocytes and hematopoietic stem cells.

In addition to direct detrimental effects of high ROS and DNA damage levels, recent data have demonstrated that chronic infection and cancer can trigger terminal differentiation and T cell exhaustion (Wherry, 2011). Therefore we evaluated the expression of various exhaustion markers associated with terminal differentiation in metabolically-sorted cells. We found that multiple negative coinhibitory receptors such as PD-1, CTLA-4, LAG-3, and BTLA that regulate T cell exhaustion were enriched at both the RNA (Figure 5F) and protein levels (Figure 5G) in the high-ΔΨm T cells compared with the low-ΔΨm T cells. The expression of multiple negative inhibitory receptors in high-ΔΨm T cells may contribute to the observed reduced long-term survival. Additionally, high-ΔΨm CD8$^+$ T cells underwent increased cell death compared with low-ΔΨm CD8$^+$ T cells, as evidenced by increased expression of the proapoptotic gene *Bax* (Figure 5H) and increased Annexin V staining (Figure 5I). These results demonstrate that high-ΔΨm cells display increased oxidative stress, DNA damage response, cell-cycle arrest, and molecular features of T cell exhaustion, each of which predispose T cells to apoptotic death. In contrast, we demonstrate that low-ΔΨm cells are more efficiently suited to combat oxidative stress, are protected from DNA damage, and are resistant to apoptosis.

Interleukin-2 Augments ΔΨm through mTOR Signaling

The presence of inflammatory cytokines (Chang et al., 2014; Finlay et al., 2012; Kaech and Cui, 2012) and increased mTOR activity (Araki et al., 2009; Chi, 2012; Kaech and Cui, 2012; Shi et al., 2011; Shrestha et al., 2014) are both required for the full differentiation of functional effector T cells. Whether these cytokines regulate ΔΨm, however, remains unknown. The presence of the cytokine interleukin-2 (IL-2) during T cell priming increased the basal OCR and ΔΨm in a concentration-dependent fashion (Figures S5A and S5B). We found that low-ΔΨm cells displayed reduced activity of mTORC1 signaling, as evidenced by reduced level of phosphorylation of 4-E-BP1 and S6 phosphorylation compared to their high-ΔΨm counterparts (Figure S5C). We next tested whether the reduction of mTORC1 signaling using the mTOR inhibitor, rapamycin, would reduce ΔΨm. T cell priming in the presence of rapamycin significantly reduced ΔΨm in CD8$^+$ T cells (Figure S5D). Our results suggest that the presence of IL-2 and increase in mTORC1 signaling may increase ΔΨm to regulate the effector T cell response.

T cell differentiation is characterized by an increase in mitochondrial metabolism (Sena et al., 2013). Our data suggest that increase in ΔΨm and ROS generation are dependent on the IL2-mTOR axis. Our assertion that differences in ΔΨm may regulate cell-fate decisions was further supported by recent observations that increased mitochondrial metabolism and ROS are important for adipocyte differentiation (Tormos et al., 2011), T cell differentiation (Sena et al., 2013; Shrestha et al., 2014; Weinberg et al., 2015), and differentiation of embryonic stem cells (Schieke et al., 2008).

Low-ΔΨm CD8$^+$ T Cells Demonstrate Long-Term In Vivo Persistence and Superior Antitumor Activity

The metabolic, biochemical, and transcriptional profiles of low-ΔΨm T cells suggest that these cells might have significant

Figure 5. Low-ΔΨm CD8$^+$ T Cells Demonstrate Decreased Oxidative Stress, Increased Long-Term In Vivo Persistence, and Superior Antitumor Activity

(A) DNA damage in DAPI stained (blue) ΔΨm-sorted CD8$^+$ T cells using indirect immunofluorescence staining (green) for γ-H2A histone family member X (γ-H2AX). Bottom right shows percentage of cells with H2AX foci per high-powered field.

(B and C) Quantitative RT-PCR analysis of genes associated with (B) DNA repair and (C) cell cycle inhibition in CD8$^+$ T cells.

(D) Flow cytometric analysis for reactive oxygen species (ROS) levels using 2′,7′–dichlorofluorescein diacetate (DCFDA) fluorescence expressed in arbitrary units (AU) ΔΨm-sorted subsets.

(E) Flow cytometric analysis of DNA damage using phospho-Histone H2A.X (Ser139) antibody in ΔΨm-sorted subsets.

(F and G) (F) Quantitative RT-PCR expression levels of indicated exhaustion factors and (G) flow cytometric analysis of exhaustion markers in ΔΨm-sorted bulk CD8$^+$ T cells. Numbers in (G) indicate MFI.

(H) Quantitative RT-PCR expression levels of indicated proapoptotic gene (*Bax*) within ΔΨm-sorted bulk CD8$^+$ T cells.

(I) Representative flow cytometry analysis of Annexin and PI staining in ΔΨm-sorted bulk CD8$^+$ T cells.

Data are presented as mean ± SEM and *$p < 0.05$; **$p < 0.01$; ***$p < 0.001$; ****$p < 0.0001$ (two-tailed t test).

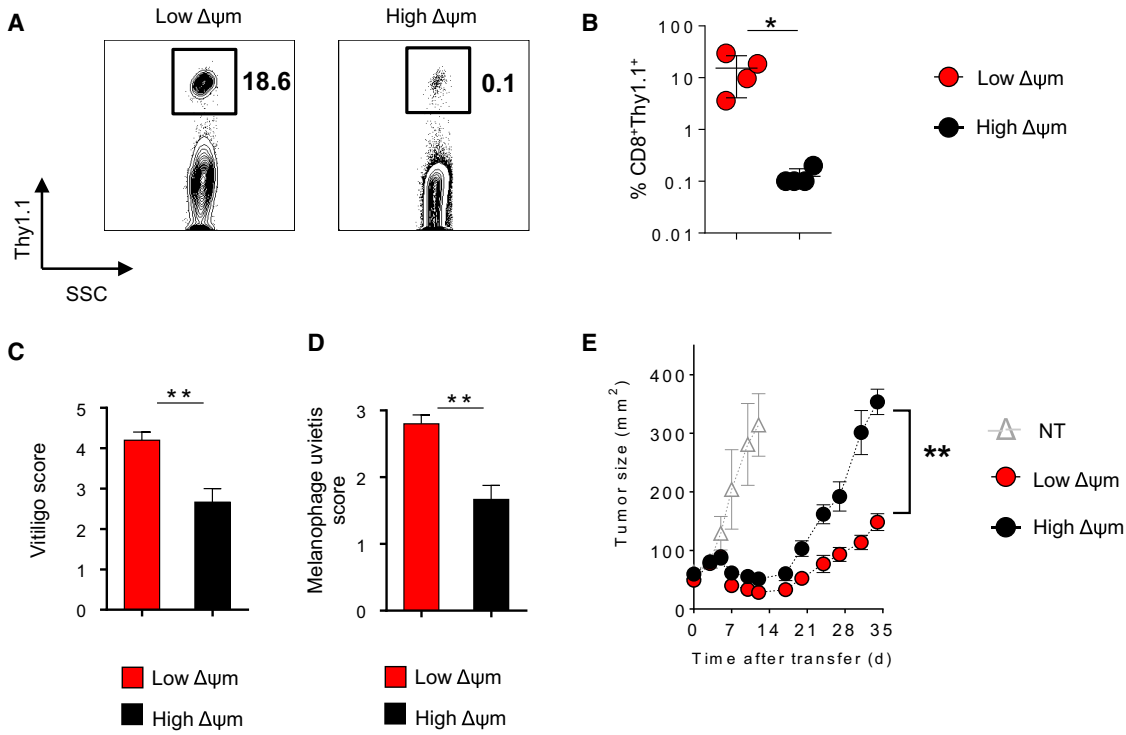

Figure 6. Low-ΔΨm CD8$^+$ T Cells Demonstrate Increased Long-Term In Vivo Persistence and Superior Antitumor Activity

(A and B) Flow cytometric analysis and quantification of persistence of transferred Thy1.1$^+$ CD8$^+$ T cells 300 days after adoptive transfer of 10^5 high-ΔΨm and low-ΔΨm cells in sublethally irradiated mice (mean ± SEM of four mice).

(C and D) Vitiligo scores and melanophage uveitis scoring in mice that received ΔΨm CD8$^+$ T cell subsets.

(E) Adoptive transfer of 10^6 high-ΔΨm or low-ΔΨm cells and subsequent infection with gp100-vaccinia virus in sublethally irradiated mice bearing 10 day established subcutaneous B16 tumors (n = 5 mice per group).

Data are presented as mean ± SEM and *$p < 0.05$; **$p < 0.01$ (two-tailed t test). (E) **$p = 0.009$ (Wilcoxon rank sum).

advantages in long-term functional reconstitution assays. Long-term persistence is one of the key biological characteristics of memory T cells (Chang et al., 2014; Graef et al., 2014; Kaech and Cui, 2012). We therefore sought to evaluate long-term survival following adoptive transfer of an equal number of low-ΔΨm and high-ΔΨm CD8$^+$ T cells. When assessed 300 days after adoptive transfer, low-ΔΨm CD8$^+$ cells displayed a dramatic increase in persistence compared with high-ΔΨm cells, as determined by the frequency and number of pmel-1 T cells in the spleen (Figures 6A and 6B). Long-term persistence of pmel-1 CD8$^+$ T cells was associated with expected on-target autoimmune sequelae through sustained damage to melanocytes. This melanocyte targeting led to the development of vitiligo, a condition that was significantly greater in recipient mice receiving low-ΔΨm cells (Figure 6C). We have also previously demonstrated that there is a strong correlation between the functionality of CD8$^+$ T cells targeting gp100 and the degree of ocular autoimmunity (Palmer et al., 2008). Therefore, we analyzed the extent of ocular injury in recipient animals 300 days after transfer. We noted that animals receiving low-ΔΨm CD8$^+$ T cells exhibited more severe uveitis when compared to the recipients of high-ΔΨm cells (Figure 6D). The ability of T cells to robustly proliferate and persist after transfer has been shown to be critical to antitumor responses in mice and humans receiving adoptive T cell-based therapies (Gattinoni et al., 2009; Sukumar et al., 2013). To test the antitumor effect of ΔΨm-sorted T cells, we adoptively transferred low-ΔΨm and high-ΔΨm T cell subsets into wild-type mice bearing subcutaneous syngeneic, large vascularized established B16 melanomas. Consistent with their memory phenotype, low-ΔΨm pmel-1 CD8$^+$ T cells displayed significantly improved in vivo antitumor functionality and mediated improved tumor regression (Figure 6E). Thus, metabolic sorting based on low mitochondrial membrane potential can identify, within a given population, a subset of T cells with high capacity for self-renewal and long-term survival as immune memory. Consistent with their stem-like characterisitcs, these low-ΔΨm T cells also have the abity to differentiate in vivo into highly potent effector cells that can mediate autoimmune tissue damage and control large, established tumors.

Characterization of ΔΨm in Human CD8$^+$ T Cells

We next evaluated whether characterizing lymphocytes in the circulation of healthy human donors (HDs) based on ΔΨm could identify less-differentiated human lymphocyte populations. We analyzed the CD8$^+$ T cells within the peripheral blood mononuclear cells (PBMCs) from healthy donors and found that low-ΔΨm sorting enriched for primarily naive CD8$^+$ T cells (CD8$^+$CD45RO$^-$CCR7$^+$) compared with high-ΔΨm-sorted CD8$^+$ T cells (Figures 7A–7C). To further test whether sorting

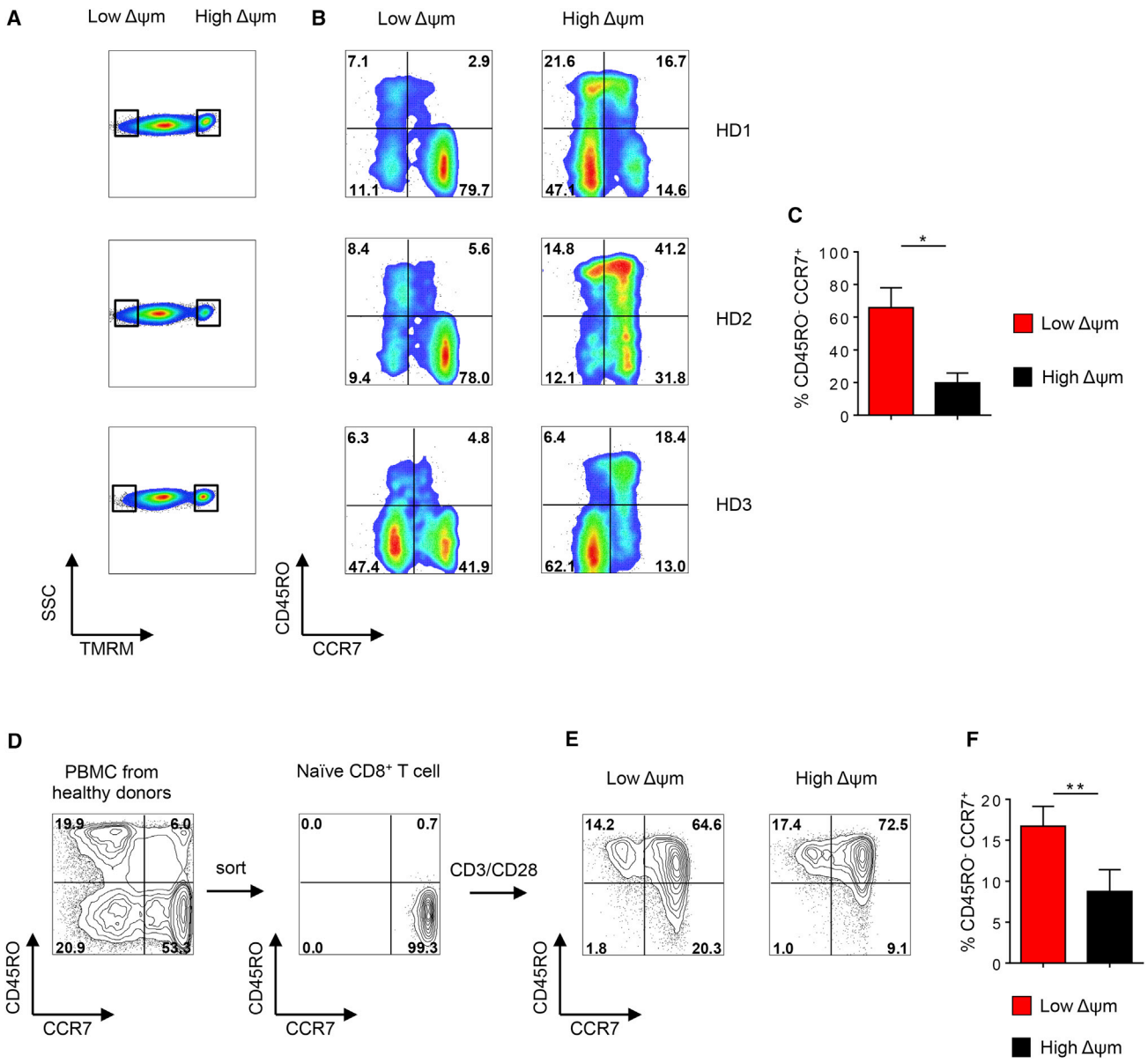

Figure 7. Low-ΔΨm Enriches for Increased Expression of CD45RO⁻CCR7⁺ in Human CD8⁺ T Cells

(A and B) Flow cytometric analysis of low-ΔΨm and high-ΔΨm human CD8⁺ T cell for CD45RO and CCR7 from peripheral blood from healthy donors.

(C) Quantification of CD45RO⁻CCR7⁺ human CD8⁺ T cells within ΔΨm subsets in three healthy donors.

(D) Representative FACS plot of purification of the naive CD8⁺ T cell subset from PBMC in a healthy donor.

(E and F) (E) Characterization and (F) quantification of activated human CD8⁺ T cells for phenotypic markers such as CD45RO and CCR7 in ΔΨm CD8⁺ T cells from four healthy donors.

Data are presented as mean ± SEM and $^{*}p < 0.05$; $^{**}p < 0.01$ (two-tailed t test paired).

activated human CD8⁺ T cells based on ΔΨm could enrich for a less-differentiated T cell subset, we purified naive CD8⁺ T cells from four healthy donors (Figure 7D) and stimulated them in vitro for 2 weeks before measuring ΔΨm. We found a 2-fold enrichment of the CD8⁺CD45RO⁻CCR7⁺ population in the low-ΔΨm subset compared with the high-ΔΨm CD8⁺ T cell subset (Figures 7E and 7F). Collectively, these data are consistent with our mouse data demonstrating that ΔΨm-based sorting can allow for the enrichment of a less-differentiated lymphocyte population.

In this study, we describe a simple and clinically feasible method to isolate metabolically robust T cells and LT-HSC for adoptive transfer. The key feature of this approach is its use of a single parameter—ΔΨm—to identify cells with global metabolic features that are critical for potent and sustained antitumor immunity and hematopoietic reconstitution. More specifically, our findings demonstrate (1) low-ΔΨm T cells more robustly express genes encoding factors known to promote memory CD8⁺ T cell formation and display the metabolic signature of increased

free fatty acid levels, increased spare respiratory capacity, and reduced glycolysis; (2) low-ΔΨm is a metabolic marker of self-renewal; (3) low-ΔΨm cells exhibit decreased oxidative stress as evidenced by reduced levels of ROS and DNA-damage—properties associated with improved functionality within other populations; and (4) metabolic sorting for low-ΔΨm T cells substantially improves long-term cellular engraftment and, in the case of tumor-reactive T cells, identifies the subset with superior therapeutic activity in vivo.

It is important to point out that measuring ΔΨm for stemness is context dependent. Specifically, cancer stem cells and iPSCs have both been found to be characterized by high ΔΨm (Folmes et al., 2011; Ye et al., 2011). However, we found that stem cell-like characteristics were associated with low-ΔΨm in LT-HSC and T cells, which have been previously shown to share many developmental attributes (Luckey et al., 2006). Transfer of low-ΔΨm HSC and $CD8^+$ T cells results in long-term reconstitution activity and persistence in vivo. It is possible that the bioenergetic profile of low-ΔΨm cells may dramatically differ during in vitro and in vivo settings. In the case of $CD8^+$ T cells, low-ΔΨm $CD8^+$ T cells in vitro display metabolic profile of long-lived T cells (decreased glycolysis and increased mitochondrial SRC). It is also possible that the metabolic state of low-ΔΨm cells may be coupled to a reprogramming of the epigenome (Lu and Thompson, 2012), resulting in persistent alterations in functional parameters even if the cell's metabolic state subsequently changes. We speculate that the increased levels of ribulose-5-phosphate derived from pentose phosphate pathway and large reserve pool of glutathione observed within the low-ΔΨm $CD8^+$ T cells may contribute to their in vivo expansion and a more favorable redox balance compared to their high-ΔΨm $CD8^+$ T cells. However, upon adoptive transfer, low-ΔΨm $CD8^+$ T cells may increase their ΔΨm and reprogram to glycolytic metabolism in vivo to support T cell expansion, persistence, and sustain effector function that are required for efficient T cell-mediated tumor clearance.

Previous efforts to identify potent antitumor T cells for adoptive transfer have largely focused on cell-surface phenotypic features characteristic of long-lived memory T cells, or have relied on functional assays, such as interferon-γ release after coculture with autologous tumor. Recent findings, however, have highlighted the importance of metabolic programs in promoting T cell survival and effector function (Chang et al., 2013; Doedens et al., 2013; Gerriets et al., 2015; Macintyre et al., 2014; MacIver et al., 2011; O'Sullivan et al., 2014; Sena et al., 2013; Shi et al., 2011). We show here that the use of ΔΨm to enrich for cells with superior metabolic features was observed even within central memory (T_{CM}), effector T cells (Tc17, Th1, Th17), and (LT-HSC). Thus, the use of metabolic sorting based on ΔΨm not only serves as a surrogate to identify long-lived memory T cells, but may provide a complementary strategy to enrich for superior cells within a wide array of phenotypically defined, clinically useful, cellular subsets. This metabolism-based approach to selecting cells for therapy may have applicability in a variety of clinical settings, including cells gene engineered with chimeric antigen receptors (CAR) or T cell receptors (TCR), that rely on the adoptive transfer strategies.

EXPERIMENTAL PROCEDURES

Mice and Tumor Lines

pmel-1 Thy-1.1 (B6.Cg-Thy-1a/Cy Tg [TcraTcrb] 8Rest/J), *Rag2*$^{-/-}$, *BwRag1*$^{-/-}$TRP-1, and C57BL/6 mice were obtained from the Jackson Laboratory. We crossed pmel-1 with Ly5.1 mice (B6.SJL-Ptprc^a*Pepc*^{b}/BoyJ) to obtain pmel-1 Ly5.1 mice. B16 (H-2D^b), a gp100$^+$ murine melanoma, was obtained from the National Cancer Institute Tumor Repository and maintained in culture media as described previously (Gattinoni et al., 2009).

Mitochondrial Membrane Potential Sorting

$CD8^+$ T cells from pmel-1 mice were stimulated in vitro with 1 μM hgp100$_{25–33}$ peptide and expanded for 4 days in culture medium containing 10 ng•ml^{-1} IL-2 (Chiron). Membrane potential was assessed using the potentiometric dye tetramethyl rhodamine methyl ester (TMRM; Sigma Aldrich) at a final concentration of 25 nm for 30 min at 37°C. For sorting of cells with different ΔΨm, $CD8^+$ gated cells were sorted into two pools corresponding to the cells with the lowest (7%–10%) and highest (7%–10%) TMRM fluorescence. Cell sorting was performed with a FACS Aria instrument (BD Biosciences). Generation of Tcm, Th1, Th17, and LT-HSC ΔΨm subsets was described in Supplemental Experimental Procedures.

Adoptive Cell Transfer and Tumor Experiments

Tumor experiments were performed as previously described (Gattinoni et al., 2009). Unless otherwise indicated, mice ($n \geq 5$ per group) were injected s.c. with 2–5 × 10^5 B16 melanoma cells. Ten to fourteen days later, treated mice received i.v. injections of pmel-1 $CD8^+$ T cells sorted based on ΔΨm and indicated doses of recombinant vaccinia virus expressing hgp100. Treated mice received 500 cGy of sublethal irradiation prior to ACT. In addition to vaccination, all treated mice also received i.p. injections of rhIL-2 administered twice daily for 3 days after transfer.

Extracellular Acidification Rate and Basal Oxygen Consumption Rate

OCR and ECAR were measured at 37°C using an XF24 extracellular analyzer (Seahorse Bioscience) as previously described (van der Windt et al., 2012). Oxygen consumption rates (OCR) and extracellular acidification rates (ECAR) were measured in XF media (nonbuffered RPMI 1640 containing 25 mM glucose, 2 mM L-glutamine, and 1 mM sodium pyruvate) under basal conditions and in response to 1 μM oligomycin, 2.0 μM fluoro-carbonyl cyanide phenylhydrazone (FCCP), or 100 nM rotenone with 1 μM antimycin A (Sigma).

Real-Time RT-PCR

We isolated RNA with the RNeasy mini kit (QIAGEN) and generated cDNA by reverse transcription (Applied Biosystems). Real-time RT-PCR was performed for all genes with primers from Applied Biosystems by Prism 7900HT (Applied Biosystems). Gene expression was calculated relative to *Actb* expression.

Intracellular ROS Measurements

For analysis of intracellular ROS, CD8+ T cells were incubated with 5 μM dichlorofluorescein diacetate (DCFDA, Invitrogen). Cells were incubated on a shaker at 37 °C for 30 min, followed immediately by flow cytometry analysis using a LSRII instrument (Becton Dickinson).

Statistics

A two-tailed Student's t test was used for comparison of data such as gene expression levels. For tumor measurements, the products of perpendicular tumor diameters were plotted as the mean ± SEM for each data point, and tumor treatment graphs were compared by using the Wilcoxon rank sum test. For all analyses, a p value less than 0.05 was considered statistically significant. For HSC in vivo reconstitution, we used a two-way ANOVA to compare treatment groups. Prism GraphPad software (GraphPad Software Inc.) was used for these analyses. *$p < 0.05$; **$p < 0.01$; ***$p < 0.001$; ****$p < 0.0001$ (two-tailed t test).

See the Supplemental Experimental Procedures.

ACCESSION NUMBERS

Microarray data comparing the T_{SCM} and T_{EM} subsets are available in NCBI GEO database under accession number GSE67825. The RNA seq data are under GEO accession number GSE74001.

SUPPLEMENTAL INFORMATION

Supplemental Information includes five figures, Supplemental Experimental Procedures, and two tables and can be found with this article at http://dx.doi.org/10.1016/j.cmet.2015.11.002.

AUTHOR CONTRIBUTIONS

M.S. designed the project. M.S., J.L., S.J.P., G.U.M., C.A.K., G.D.W, Y.J., S.M., L.G., and P.M. performed experiments. M.S., J.L., S.J.P., C.A.K., Y.J., P.L., G.D.W., Z.Y., K.K., M.R., E.W., F.M., P.M., and L.G. analyzed data. M.S., G.U.M., S.P., J.G.C., C.A.K., P.L., R.R., D.P., D.C., R.L.E., D.S., W.L., P.M., T.F., and N.P.R. edited the manuscript. M.S and N.P.R. wrote the manuscript.

ACKNOWLEDGMENTS

This research was supported with gifts from the Milstein Family Foundation and Mr. Jinyuan Li, chairman of the Tiens Charitable Foundation; by the Leducq Foundation; and by the Intramural Research Programs of the NCI and NHLBI. We thank A. Mixon and S. Farid of the Flow Cytometry Unit for help with sorting, and D. Goldstein and M. Malik for help with Metabolon. We thank Steven A. Rosenberg for his support. This study was done in partial fulfillment of a PhD in Biomedical Sciences (to S.J.P.) at Georgetown University.

Received: April 20, 2015
Revised: September 7, 2015
Accepted: November 4, 2015
Published: December 3, 2015

REFERENCES

Araki, K., Turner, A.P., Shaffer, V.O., Gangappa, S., Keller, S.A., Bachmann, M.F., Larsen, C.P., and Ahmed, R. (2009). mTOR regulates memory CD8 T-cell differentiation. Nature *460*, 108–112.

Berod, L., Friedrich, C., Nandan, A., Freitag, J., Hagemann, S., Harmrolfs, K., Sandouk, A., Hesse, C., Castro, C.N., Bähre, H., et al. (2014). De novo fatty acid synthesis controls the fate between regulatory T and T helper 17 cells. Nat. Med. *20*, 1327–1333.

Brentjens, R.J., Davila, M.L., Riviere, I., Park, J., Wang, X., Cowell, L.G., Bartido, S., Stefanski, J., Taylor, C., Olszewska, M., et al. (2013). CD19-targeted T cells rapidly induce molecular remissions in adults with chemotherapy-refractory acute lymphoblastic leukemia. Sci. Transl. Med. *5*, 177ra38.

Chang, C.H., Curtis, J.D., Maggi, L.B., Jr., Faubert, B., Villarino, A.V., O'Sullivan, D., Huang, S.C., van der Windt, G.J., Blagih, J., Qiu, J., et al. (2013). Posttranscriptional control of T cell effector function by aerobic glycolysis. Cell *153*, 1239–1251.

Chang, J.T., Wherry, E.J., and Goldrath, A.W. (2014). Molecular regulation of effector and memory T cell differentiation. Nat. Immunol. *15*, 1104–1115.

Chi, H. (2012). Regulation and function of mTOR signalling in T cell fate decisions. Nat. Rev. Immunol. *12*, 325–338.

Doedens, A.L., Phan, A.T., Stradner, M.H., Fujimoto, J.K., Nguyen, J.V., Yang, E., Johnson, R.S., and Goldrath, A.W. (2013). Hypoxia-inducible factors enhance the effector responses of CD8(+) T cells to persistent antigen. Nat. Immunol. *14*, 1173–1182.

Ehrenberg, B., Montana, V., Wei, M.D., Wuskell, J.P., and Loew, L.M. (1988). Membrane potential can be determined in individual cells from the nernstian distribution of cationic dyes. Biophys. J. *53*, 785–794.

Finlay, D.K., Rosenzweig, E., Sinclair, L.V., Feijoo-Carnero, C., Hukelmann, J.L., Rolf, J., Panteleyev, A.A., Okkenhaug, K., and Cantrell, D.A. (2012). PDK1 regulation of mTOR and hypoxia-inducible factor 1 integrate metabolism and migration of CD8+ T cells. J. Exp. Med. *209*, 2441–2453.

Folmes, C.D., Nelson, T.J., Martinez-Fernandez, A., Arrell, D.K., Lindor, J.Z., Dzeja, P.P., Ikeda, Y., Perez-Terzic, C., and Terzic, A. (2011). Somatic oxidative bioenergetics transitions into pluripotency-dependent glycolysis to facilitate nuclear reprogramming. Cell Metab. *14*, 264–271.

Gattinoni, L., Finkelstein, S.E., Klebanoff, C.A., Antony, P.A., Palmer, D.C., Spiess, P.J., Hwang, L.N., Yu, Z., Wrzesinski, C., Heimann, D.M., et al. (2005). Removal of homeostatic cytokine sinks by lymphodepletion enhances the efficacy of adoptively transferred tumor-specific CD8+ T cells. J. Exp. Med. *202*, 907–912.

Gattinoni, L., Zhong, X.S., Palmer, D.C., Ji, Y., Hinrichs, C.S., Yu, Z., Wrzesinski, C., Boni, A., Cassard, L., Garvin, L.M., et al. (2009). Wnt signaling arrests effector T cell differentiation and generates CD8+ memory stem cells. Nat. Med. *15*, 808–813.

Gerriets, V.A., and Rathmell, J.C. (2012). Metabolic pathways in T cell fate and function. Trends Immunol. *33*, 168–173.

Gerriets, V.A., Kishton, R.J., Nichols, A.G., Macintyre, A.N., Inoue, M., Ilkayeva, O., Winter, P.S., Liu, X., Priyadharshini, B., Slawinska, M.E., et al. (2015). Metabolic programming and PDHK1 control CD4+ T cell subsets and inflammation. J. Clin. Invest. *125*, 194–207.

Graef, P., Buchholz, V.R., Stemberger, C., Flossdorf, M., Henkel, L., Schiemann, M., Drexler, I., Höfer, T., Riddell, S.R., and Busch, D.H. (2014). Serial transfer of single-cell-derived immunocompetence reveals stemness of CD8(+) central memory T cells. Immunity *41*, 116–126.

Ito, K., Carracedo, A., Weiss, D., Arai, F., Ala, U., Avigan, D.E., Schafer, Z.T., Evans, R.M., Suda, T., Lee, C.H., and Pandolfi, P.P. (2012). A PML–PPAR-δ pathway for fatty acid oxidation regulates hematopoietic stem cell maintenance. Nat. Med. *18*, 1350–1358.

June, C.H., Riddell, S.R., and Schumacher, T.N. (2015). Adoptive cellular therapy: a race to the finish line. Sci. Transl. Med. *7*, 280ps7.

Kaech, S.M., and Cui, W. (2012). Transcriptional control of effector and memory CD8+ T cell differentiation. Nat. Rev. Immunol. *12*, 749–761.

Lu, C., and Thompson, C.B. (2012). Metabolic regulation of epigenetics. Cell Metab. *16*, 9–17.

Luckey, C.J., Bhattacharya, D., Goldrath, A.W., Weissman, I.L., Benoist, C., and Mathis, D. (2006). Memory T and memory B cells share a transcriptional program of self-renewal with long-term hematopoietic stem cells. Proc. Natl. Acad. Sci. USA *103*, 3304–3309.

Macintyre, A.N., Gerriets, V.A., Nichols, A.G., Michalek, R.D., Rudolph, M.C., Deoliveira, D., Anderson, S.M., Abel, E.D., Chen, B.J., Hale, L.P., and Rathmell, J.C. (2014). The glucose transporter Glut1 is selectively essential for CD4 T cell activation and effector function. Cell Metab. *20*, 61–72.

MacIver, N.J., Blagih, J., Saucillo, D.C., Tonelli, L., Griss, T., Rathmell, J.C., and Jones, R.G. (2011). The liver kinase B1 is a central regulator of T cell development, activation, and metabolism. J. Immunol. *187*, 4187–4198.

MacIver, N.J., Michalek, R.D., and Rathmell, J.C. (2013). Metabolic regulation of T lymphocytes. Annu. Rev. Immunol. *31*, 259–283.

Michalek, R.D., Gerriets, V.A., Jacobs, S.R., Macintyre, A.N., MacIver, N.J., Mason, E.F., Sullivan, S.A., Nichols, A.G., and Rathmell, J.C. (2011a). Cutting edge: distinct glycolytic and lipid oxidative metabolic programs are essential for effector and regulatory CD4+ T cell subsets. J. Immunol. *186*, 3299–3303.

Michalek, R.D., Gerriets, V.A., Nichols, A.G., Inoue, M., Kazmin, D., Chang, C.Y., Dwyer, M.A., Nelson, E.R., Pollizzi, K.N., Ilkayeva, O., et al. (2011b). Estrogen-related receptor-α is a metabolic regulator of effector T-cell activation and differentiation. Proc. Natl. Acad. Sci. USA *108*, 18348–18353.

Morita, Y., Ema, H., and Nakauchi, H. (2010). Heterogeneity and hierarchy within the most primitive hematopoietic stem cell compartment. J. Exp. Med. *207*, 1173–1182.

Muranski, P., Borman, Z.A., Kerkar, S.P., Klebanoff, C.A., Ji, Y., Sanchez-Perez, L., Sukumar, M., Reger, R.N., Yu, Z., Kern, S.J., et al. (2011). Th17 cells are long lived and retain a stem cell-like molecular signature. Immunity *35*, 972–985.

O'Sullivan, D., van der Windt, G.J., Huang, S.C., Curtis, J.D., Chang, C.H., Buck, M.D., Qiu, J., Smith, A.M., Lam, W.Y., DiPlato, L.M., et al. (2014). Memory CD8(+) T cells use cell-intrinsic lipolysis to support the metabolic programming necessary for development. Immunity *41*, 75–88.

Palmer, D.C., Chan, C.C., Gattinoni, L., Wrzesinski, C., Paulos, C.M., Hinrichs, C.S., Powell, D.J., Jr., Klebanoff, C.A., Finkelstein, S.E., Fariss, R.N., et al. (2008). Effective tumor treatment targeting a melanoma/melanocyte-associated antigen triggers severe ocular autoimmunity. Proc. Natl. Acad. Sci. USA *105*, 8061–8066.

Pearce, E.L., Walsh, M.C., Cejas, P.J., Harms, G.M., Shen, H., Wang, L.S., Jones, R.G., and Choi, Y. (2009). Enhancing CD8 T-cell memory by modulating fatty acid metabolism. Nature *460*, 103–107.

Pearce, E.L., Poffenberger, M.C., Chang, C.H., and Jones, R.G. (2013). Fueling immunity: insights into metabolism and lymphocyte function. Science *342*, 1242454.

Porter, D.L., Levine, B.L., Kalos, M., Bagg, A., and June, C.H. (2011). Chimeric antigen receptor-modified T cells in chronic lymphoid leukemia. N. Engl. J. Med. *365*, 725–733.

Restifo, N.P., Dudley, M.E., and Rosenberg, S.A. (2012). Adoptive immunotherapy for cancer: harnessing the T cell response. Nat. Rev. Immunol. *12*, 269–281.

Riddell, S.R., and Greenberg, P.D. (1995). Principles for adoptive T cell therapy of human viral diseases. Annu. Rev. Immunol. *13*, 545–586.

Schieke, S.M., Ma, M., Cao, L., McCoy, J.P., Jr., Liu, C., Hensel, N.F., Barrett, A.J., Boehm, M., and Finkel, T. (2008). Mitochondrial metabolism modulates differentiation and teratoma formation capacity in mouse embryonic stem cells. J. Biol. Chem. *283*, 28506–28512.

Sena, L.A., Li, S., Jairaman, A., Prakriya, M., Ezponda, T., Hildeman, D.A., Wang, C.R., Schumacker, P.T., Licht, J.D., Perlman, H., et al. (2013). Mitochondria are required for antigen-specific T cell activation through reactive oxygen species signaling. Immunity *38*, 225–236.

Shi, L.Z., Wang, R., Huang, G., Vogel, P., Neale, G., Green, D.R., and Chi, H. (2011). HIF1alpha-dependent glycolytic pathway orchestrates a metabolic checkpoint for the differentiation of TH17 and Treg cells. J. Exp. Med. *208*, 1367–1376.

Shrestha, S., Yang, K., Wei, J., Karmaus, P.W., Neale, G., and Chi, H. (2014). Tsc1 promotes the differentiation of memory CD8+ T cells via orchestrating the transcriptional and metabolic programs. Proc. Natl. Acad. Sci. USA *111*, 14858–14863.

Simsek, T., Kocabas, F., Zheng, J., Deberardinis, R.J., Mahmoud, A.I., Olson, E.N., Schneider, J.W., Zhang, C.C., and Sadek, H.A. (2010). The distinct metabolic profile of hematopoietic stem cells reflects their location in a hypoxic niche. Cell Stem Cell *7*, 380–390.

Suda, T., Takubo, K., and Semenza, G.L. (2011). Metabolic regulation of hematopoietic stem cells in the hypoxic niche. Cell Stem Cell *9*, 298–310.

Sukumar, M., Liu, J., Ji, Y., Subramanian, M., Crompton, J.G., Yu, Z., Roychoudhuri, R., Palmer, D.C., Muranski, P., Karoly, E.D., et al. (2013). Inhibiting glycolytic metabolism enhances CD8+ T cell memory and antitumor function. J. Clin. Invest. *123*, 4479–4488.

Takubo, K., Goda, N., Yamada, W., Iriuchishima, H., Ikeda, E., Kubota, Y., Shima, H., Johnson, R.S., Hirao, A., Suematsu, M., and Suda, T. (2010). Regulation of the HIF-1alpha level is essential for hematopoietic stem cells. Cell Stem Cell *7*, 391–402.

Tormos, K.V., Anso, E., Hamanaka, R.B., Eisenbart, J., Joseph, J., Kalyanaraman, B., and Chandel, N.S. (2011). Mitochondrial complex III ROS regulate adipocyte differentiation. Cell Metab. *14*, 537–544.

van der Windt, G.J., Everts, B., Chang, C.H., Curtis, J.D., Freitas, T.C., Amiel, E., Pearce, E.J., and Pearce, E.L. (2012). Mitochondrial respiratory capacity is a critical regulator of CD8+ T cell memory development. Immunity *36*, 68–78.

Wang, R., and Green, D.R. (2012). Metabolic checkpoints in activated T cells. Nat. Immunol. *13*, 907–915.

Weinberg, S.E., Sena, L.A., and Chandel, N.S. (2015). Mitochondria in the regulation of innate and adaptive immunity. Immunity *42*, 406–417.

Wherry, E.J. (2011). T cell exhaustion. Nat. Immunol. *12*, 492–499.

Ye, X.Q., Wang, G.H., Huang, G.J., Bian, X.W., Qian, G.S., and Yu, S.C. (2011). Heterogeneity of mitochondrial membrane potential: a novel tool to isolate and identify cancer stem cells from a tumor mass? Stem Cell Rev. *7*, 153–160.